Rowan University

Rowan Digital Works

Theses and Dissertations

8-27-2020

Bioprinted in vitro model of human glioblastoma

Rachel Lauren Schwartz
Rowan University

Follow this and additional works at: https://rdw.rowan.edu/etd

 Part of the Biomedical Engineering and Bioengineering Commons, and the Mechanical Engineering Commons

Let us know how access to this document benefits you - share your thoughts on our feedback form.

Recommended Citation

Schwartz, Rachel Lauren, "Bioprinted in vitro model of human glioblastoma" (2020). *Theses and Dissertations*. 2837.
https://rdw.rowan.edu/etd/2837

BIOPRINTED IN VITRO MODEL OF HUMAN GLIOBLASTOMA

by

Rachel L. Schwartz

A Thesis

Submitted to the
Department of Mechanical Engineering
College of Engineering
In partial fulfillment of the requirement
For the degree of
Master of Science in Mechanical Engineering
at
Rowan University
July 13, 2020

Thesis Chairs: Amir K. Miri, PhD; Gary Thompson, PhD

Dedication

I would like to dedicate this manuscript to my parents Janet and Michael Schwartz for all

the support and encouragement they have given me.

Abstract

Rachel L. Schwartz
BIOPRINTED IN VITRO MODEL OF HUMAN GLIOBLASTOMA
2018-2020
Amir K. Miri, PhD, Gary Thompson, PhD
Master of Science in Mechanical Engineering

Glioblastoma multiform (GBM) is one of the most aggressive forms of primary brain tumors. GBM is fast progressing and resistant to treatment, resulting in a low survival rate. Conventional 2-dimensional tissue culture models cannot fully replicate the complexities of cancer lesions that contain multiple cell types and structures (e.g. vessels composed of endothelial cells, cancer cells, normal cells, etc.) as well as an intricate scaffold of proteins comprising the extracellular matrix (ECM). In addition, animal models cannot translate into the clinical disease in patients. Thus, this study has developed a bioprintable organ-on-a-chip (OOAC) model that mimics the important ECM factors of the GBM tumor microenvironment to study GBM invasive migration *in vitro*. Gelatin methacrylol (GelMA), endothelial cell (HUVEC) lined channels, human GBM cells (U87) and hyaluronic acid (HA) were selected to create bioinks to print the OOAC. 5-7% (w/v). GelMA with variable levels of HA was found to be mechanically comparable to native ECM of the brain. Different bioink combinations were explored to match the Young's modulus of common GBM tumors found in literature. Spreading of endothelial cells in a microfluidic channel were observed with a monoculture OOAC, and a viable bioink composition and culture method were developed to support co-culture in the OOAC. Our diseased tissue model can replicate the GBM ECM and can allow for multi-cell culture migration studies in the future.

Table of Contents

Table of Contents (Continued)

Table of Contents (Continued)

List of Figures

List of Tables

Chapter 1

Introduction and Background

1.1. Introduction and Background

Over 1.7 million new cancer cases are diagnosed in the US each year, which is 4,700 new cancer diagnoses each day [1]. Within the past few decades, there have been discoveries in new forms of cancer treatments, understanding cancer pathways, and a broader understanding of cancer metastasis. Primary brain tumors have a high mortality rate with the most lethal sub-type being Glioblastoma multiforme (GBM), with more than 30,000 new cases every year [2], [3]. The median survival rate for patients with this disease is approximately 15 months [3]–[5]. There is a lack of proper treatments because of feasible pre-clinical models that can provide information to develop new forms of therapeutics. Engineered models have the potential to accurately mimic the GBM microenvironment outside of a patient's body, allowing for better tools for research [6].

1.1.1. Problem statement. GBM patients suffer from poor prognosis attributed to: (1) tumor location; (2) blood brain barrier and drug uptake; (3) aggressiveness; and, (4) a lack of relevant preclinical models for drug development [2], [3], [5]. Complete removal of the tumor is difficult due to the location of the tumors, as the tissue can be a part of key neurological functions and full removal is not always beneficial for quality of life [2], [5]. Results tend to be modest due the aggressive nature of GBM. This contributes to the poor prognosis of GBM, which is recognized as an orphan disease by the World Health Organization (WHO) [1], [5]

Current pre-clinical GBM studies consist of *in vitro* cell culture methods and animal models. Two-dimensional (2-D) cell culture models are relatively inexpensive and allow for real time imaging; however, they lack the three-dimensional (3-D) complexity of GBM *in vivo*. Animal models provide *in vivo* complexity that is not possible with *in vitro* monolayer models [7]–[11]. Animal models have different tissue mechanical properties and metabolism, are expensive, time consuming, and limited data points can be collected [8], [11], [12]. To address this, there has been a movement towards utilizing 3-D bioprinted models to study behavior *in vitro* [8], [13]–[17]. It has been found that for GBM, utilizing a model that has multiple cell lines and a synthetic extracellular matrix (ECM) allows for behavior similar to *in vivo* tissue [18]–[20]. For lung cancer there has been a successful model that can monitor and track invasion of cancer cells towards endothelial lined microfluidic channels that mimic malignant invasion *in vitro* [21]. There is currently no *in vitro* co-culture GBM model that mimics the ECM and invasive migration towards endothelial lined channels.

1.1.2. Significance of study. In the US, there are currently 700,000 people who are living with a brain tumor. In the year of 2020, an additional 87,240 people will receive a primary brain tumor diagnosis [22]. Of that number, 25,800 people will be diagnosed with a malignant brain tumor [22]. Only 36 % of patients will survive the 5-year treatment, and only 6.8 % of patients with GBM will survive the 5-year treatment [1], [22]. It is estimated in 2020, that 18,000 people will die from malignant brain tumors [1]. Pediatric brain tumors are also the leading cause of cancer-related death surpassing leukemia, and 4.3 % of all malignant brain tumors are diagnosed in children 0-14 years old [22]. It is the third leading cause of cancer-related death for adolescent age groups (15-29) [22].

Our OOAC has the potential to be used as a tool to monitor behavior *in vitro* that is comparable to *in vivo*. Similar OOACs for other cancer lines have been used for: a screening tool for new treatments, for toxicity testing of treatments, and in studies to understand better understand cell behavior [8], [9], [21], [23]. This model could impact the design of new treatment strategies for pharmaceutical and biomedical devices. This OOAC model would be used as an *in vitro* GBM invasive migration utilizing by replicating the ECM environment that can be monitored in real time.

1.2. Glioblastoma Multiforme

1.2.1. GBM environment. Glioblastoma is a destructive solid tumor that forms in the brain, which infiltrates into surrounding brain tissue [2], [19], [24].An important component of this tissue is the extracellular matrix (ECM). The brain ECM has a unique composition and lacks the rigid matrix of fibronectin and laminin that is typical of other tissue [25], [26]. Instead, brain intercellular spaces are filled by proteoglycans [27], [28], a class of water binding proteins produced by astrocytes and oligodendrocytes. It is formed with a network of macromolecular proteins of collagen IV and elastin; this matrix is enriched with hyaluronic acid (HA). HA contributes to structural support and regulate intracellular signaling [26], [31] and is associated with cytokines involved in proliferation and inflammation [29], [30].

The other key components of the surrounding environment are comprised of astrocytes (healthy brain cells), neurons, endothelial cells (blood vessel lining), oligodendrocytes (a part of CNS function), pericytes (outside encasement of endothelial cells), and vascular basement membrane (barrier between vascular and surrounding extra cellular matrix) [31]–[33].

Necrotic core
↓ Elastic modulus
↑ Vaso-occlusion and hypoxia
↑ Invasion from core to pseudopalisades
↑ TAMs

Pseudopalisade/ infiltrating rim
↑ Elastic modulus
↑ Matrix production
↑ Invasion at rim
↑ TAMs

Angiogenesis
↑ Leaky, poorly formed vasculature
↑ Interstitial pressure
↑ TAM infiltration
• Changes in vascular basement membrane composition

Intraparenchymal invasion
↑ Remodelling and invasion of myelinated axon tracts
↑ Interstitial fluid flow and subsequent invasion
↑ Reactive stromal cells
↑ ECM production

Perivascular space
↑ Interstitial fluid flow
↑ Nutrient availability
↑ Invasion along vascular membranes and disruption of BBB
↑ Stemness of GSCs in perivascular niche

GBM tumour cell
TAM
Neuron
Astrocyte
Endothelial cell
Oligodendrocyte
Pericyte
Vascular basement membrane
Collapsed vessel

Figure 1. Illustration showcasing the regions of tissue in a glioblastoma tumor [33]

1.2.2. Hyaluronic acid. The concentration of HA in the ECM of GBM-afflicted tissue has been found to be elevated compared to healthy brain tissue [24], [31], [34]. A contributor to this phenomenon is that glioma cells increase the amount of HA receptors, which plays a role in cell migration and invasion [29], [29], [30], [35]. The presence of HA has been shown *in vitro* to increase proliferation and invasiveness [29], [32], [36]. Common materials that have been used as a base for in vitro brain ECMs are gelatin methacrylate and hyaluronic methacrylate [11], [12], [37], [38]. Gelatin and HA are shown to provide support that the ECM typically provides as well as aid in maintaining cellular function [38], [39]. The addition of the methacrylate group to gelatin allows for the material to be crosslinked via ultraviolet light (UV), allowing for precise patterning and bypassing the thermosensitive natures of the materials [12]. The presence of HA has been found to improve the viability and function of astrocytes and GBM in vitro [35], [40], [41]. As such the presence of HA is highly desired when working on an in vitro model.

1.2.3. GBM stiffness. GBM has been found to strongly express HA and HA receptors, such as CD44 [24], [34]. It has been hypothesized that since CD44 increases proliferation, it acts in a symbiotic cycle resulting in a higher concentration of GBM cells [37], [38]. As the tumor becomes bigger, more destruction of the surrounding tissue occurs, which could cause the slightly lower mechanical properties of the tissue [22], [28], [45], [46]. Studies have been conducted on brain tissue and different forms of primary brain tumors in order to get an idea of the magnitude of changes of the mechanical properties. Young's moduli were collected from samples of cancerous and healthy brain tissue from human patients. Healthy human brain tissue has an average Young's modulus of 7.3 ± 2.1

kPa [45]. In addition to healthy brain tissue two forms of gliomas were tested: low-grade gliomas (23.7±4.9 kPa) and high-grade gliomas.

1.2.4. Blood brain barrier. Blood vessels in the brain have a highly selective and controlled barrier known as the blood brain barrier (BBB) [28], [42]. This selective barrier reflects the brain's critical roles in cognition, regulating metabolism, and coordinating the functions of peripheral organs [42], [43]. The BBB is a semipermeable border between the brain and the outside tissue. It controls ions traveling across the brain, ensuring that proper function can be maintained [27], [42]. This barrier prevents nonselective travel of solutes, cells, and toxins from accessing the CNS extracellular fluid. The BBB is a complex that surrounds most blood vessels within the brain. The first layer is comprised of tight junction endothelial cells which prevent the passage and diffusion from the blood to the surrounding space. The next basement membrane layer is comprised of pericytes and vascular smooth muscle cells (VSMCs), which incompletely surround the blood vessel. Pericytes and VSMCs provide contractile function to control vessel diameter [43]. Surrounding this layer is the basement membrane which acts as an additional barrier between the blood vessels and the ECM. The outer layer is formed with the astrocytic feet of astrocyte cells, which completely surround the blood vessels and aid in keeping the junctions tight, and which promote endothelial cells to form the BBB barrier [42]–[44]. This layered formation of blood vessels in the brain causes difficulty in drug delivery to cancer sites within the brain [27], [45].
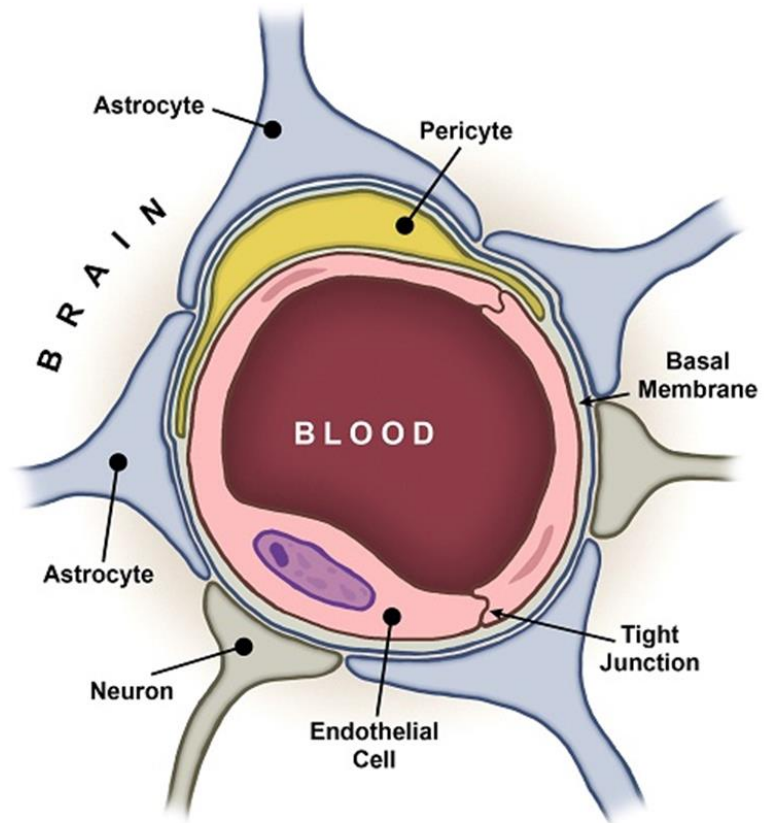
Figure 2. Exemplative illustration of a blood brain barrier [45]

1.3. *In Vitro* GBM Models

Many methodologies have been developed to address the need for research in glioblastoma multiform (GBM). These methodologies include: 2-D monoculture, multi-culture, chemical gradients, culture substrates, microfluidic models, and combinations of these factors[2], [35], [46], [47]. GBM is an aggressive form of brain cancer, as such it is important that any model developed can replicate some of the phenotype behavior observed *in vivo*. An overview follows of some of these methods and the models that were developed to replicate cancer metastasis, GBM biology, and cell-to-cell interactions.

1.3.1. 2-D GBM models. Traditional cell models are comprised of a 2-D cell culture, which is often done on glass or treated polystyrene. This stiff material encourages cells to adhere, proliferate, and move across the surface. Monoculture 2-D models have emerged to study many concerns associated with GBM[31], [35]. This method has been utilized for: whole genome sequencing [2], drug screening of GBM phenotypes, [46], implants for animal models, [48] and studying cell signaling[30], [31], [35].

1.3.2. 3-D GBM models. With the emergence of technology and understanding of cancer metastasis, there has been a push towards developing 3D models for cell culture [8], [49], [50]. One of the benefits with 3D cell culture is utilizing substrates that are biomimetic to the *in vivo* tissue environment [24], [50]. One approach often used to achieve this is a biocompatible hydrogel that has properties that are biomimetic to native tissue[11], [17], [50]. This has been shown to increase cell growth, develop a complex cellular environment, and elicit invasive behavior [15], [49], [51], [52].

1.3.3. GBM OOAC models. Many OOAC models have been produced in 2-D and 3D to try to create a better cancer model, often with a goal to capture the cancer cascade and study invasion[8], [13], [23], [47], [53].

OOAC contain a microfluidic channel in which media with nutrients are supplied to the surrounding cells [8]. Studies have shown that microfluidic flow, mechanical properties, and the presence of cells affect invasiveness [8]–[10], [19]. The presence of multiple cell lines in OOAC models have shown to better mimic the tumor microenvironment and progression of an *in vivo* environment [2], [10], [21], [23], [47], [54].

Microfluidic channels within OOAC are a critical factor to ensure in thicker 3D constructs ample nutrients and supplies are delivered throughout the system. These channels are formed through the use of molds or through the use of sacrificial material [7], [17]. Sacrificial materials that can be removed through temperature or chemical interactions are more common when developing OOAC through bioprinting [55]. This allows for small capillary-sized channels to be left within more complex structures that are more difficult to achieve via molds [55], [56].

When utilizing OOAC for co-culture systems, seeding endothelial cells within microfluidic channels with the presence of shear flow, has been shown to help form a lumen *in vitro*[21]. Endothelial lined microfluidic channels are mimetic to vasculature *in vivo* [21], [57], [58] and in co-cultures with cancer lines causes increased invasive behavior [9], [18], [44], [54].

1.4. 3-D Tissue Modeling Methods

The field of tissue engineering has emerged in recent years in order to meet the needs of 3D cell culturing. Tissue engineering is designed to model or replace different tissues in the body [8], [11], [59]. This is achieved through the use of biocompatible biomaterials, cells, or a combination of both [54], [59], [60]. Table 1 provides an overview of the main assembly methods and the related aspects of each type of tissue engineering methods [11].

Table 1

Comparison of engineering pre-clinical models [19]

Assembly Method	Materials	Resolution	Advantages	Disadvantages	Techniques
Bioprinting	Natural and Synthethic Polymers, High cell concentrations	10-1000 μm	Control of tissue geometry, rapid production, precise patterning	Technique can affect viability, limited material options	Extrusion, laser assisted, inkjet, stereolithography
Molding	Natural and Synthethic Polymers, Cell Sheets	>500 nm	Accurate small features, molds reusable, genlte on cells	Wide range of materials, controllable material	Cell sheet stacking, lithography, injection molding
Porous Scaffolds	Natural and Synthethic Poylmers, Ceramics, Metals	100nm-1000μm	Scaffolds homogenous, multiple scaffold combinations,	Less control of cell patterning, less control of scaffold geometry, can damage cells	Electrospinning, phase seperation, freeze drying, self assembly

As shown in Table 1, each method has its own advantages and disadvantages. Bioprinting has the highest resolution among the three methods, and allows for precise cell and material patterning [8], [11], [59]. In both tissue engineering and *in vitro* modeling, utilizing these microenvironments help more effectively reproduce features of an *in vivo* tissue environment compared to a classic 2-D cell culture. This method of fabrication has

10

been utilized in a large variety of applications including tissue engineering, drug delivery, oncology models, wound repair, tissue replacement, and bioreactors [8], [11], [59].

1.4.1. Bioink. In bioprinting, materials that are used for the printing process are known as bioinks. They often are biocompatible or inert polymers that are used to print for biological purposes. Common materials for bioinks consist of: alginate, gelatin, decellularized ECM, and Pluronic [11], [55], [60]. Often, bioinks need to be crosslinked in some fashion to maintain the printed shape for an *in vitro* or *in vivo* testing environment. This is accomplished through a few methods including chemical crosslinking, UV crosslinking, and thermal gelation. Chemical crosslinking is when some component of the biomaterial interacts with a chemical to crosslink the material (i.e. alginate and calcium chloride) [8], [59], [61]. In UV crosslinking, a photoinitiator (PI) is added to the bioink and exposed to a UV light, which then crosslinks the material [5]. Some common UV crosslinked bioinks are those with a methacrylate group, such as gelatin methacrylate (GelMA) or hyaluronic methacrylate (HAMA) [8], [37], [59]. UV crosslinking usually does not affect cell viability in this method [61]–[63].

1.4.2. Bioprinting approaches. Three-dimensional bioprinting may be broken down into four main categories: extrusion printing, inkjet-based printing, laser assisted printing, and photocured printing. Within each of these subcategories each have their own strengths and limitations, and are intended for different applications. All of these methods utilize some type of bioink and require some form of crosslinking. In some systems, the crosslinking is accomplished during the printing process. Other methods require crosslinking after the printing process is completed [11], [59]

11

Table 2

Comparison of bioprinting methods [65]

Parameter	Inkjet	Extrusion	Stereolithography
Speed	Medium	Low	High
Cost	Low	Low	Medium
Resolution	100-500 µm	100-500 µm	20-100 µm

1.4.3. Extrusion bioprinting. Extrusion is utilized in many forms of 3D printing. The most common place is fused deposition modeling (FDM). FDM uses heat to melt the printing material (e.g. PLA, ABS, etc.), that is then printed and cooled into the desired shape. For 3D bioprinting, this is achieved with a combination of a fluid-dispensing system and an automated motion system [8].

1.4.4. Inkjet bioprinting. Inkjet-based bioprinting is similar to 2-D inkjet printing. A bioink solution is stored within ink cartridges connected to a printer head. The material is then extruded droplet-wise by deforming the printing head. This is often done by an actuator that is squeezed to generate droplets of a controllable size [19], [28], [53], [66]. Within this bioprinting method, there are two methods in which bioink printing is achieved: continuous ink jetting and drop-on-demand.

1.4.5. Light based bioprinting. Laser-assisted bioprinting was developed from laser direct and laser-induced transfer technologies [18], [67]. Laser-assisted printing comprises of two layers: a donor layer and energy absorbing layer. The donor layer responds to a pulsed laser beam with a focusing system. This is supported by a 'ribbon' that is typically made from glass and has an energy absorbing layer (e.g. gold or titanium)

[67]–[70]. This donor layer is a part of two material layers. It is positioned on top of a bioink layer, and when the laser-assisted device pulsates on the donor layer, a high-pressure bubble is formed [68]–[70]. When this bubble is formed, the force will propel the cell-laden bioink towards a collector substrate [18], [68], [70]. Figure 3 shows an image of this process [68].
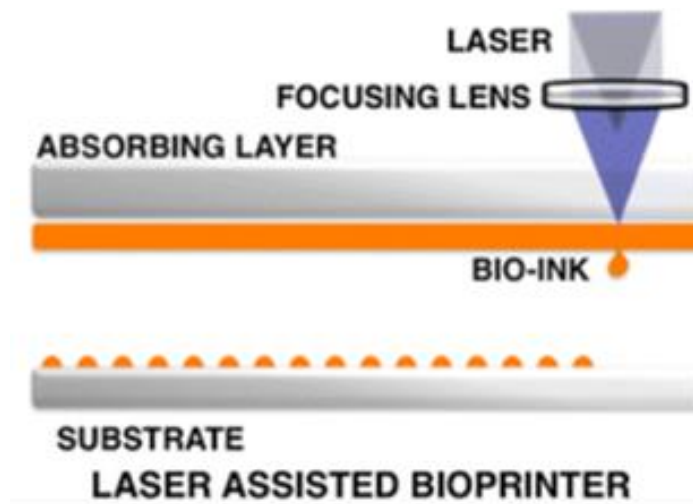
Figure 3. Diagram of laser assisted bioprinting [66]

In laser assisted bioprinting, the laser is a coherent light source. As a result, this printing process tends to be one of the most expensive. It utilizes excimer argon fluoride (ArF), krypton fluoride (KrF), or neodynmium-doped yttrium aluminum garnet (Nd: YAG) to act as a laser pulse generator. There are no devices commercially available on the market for this printing process [11], [50], [64]. This process achieves a high cell viability (>95 %), has a medium print speed (200-1,600 mm/s), and can handle a good range of viscosities [11], [65]. Cell density tends to be at a medium for the four main printing methods,

typically <108 cells/mL [11]. Due to this method being able to have high precision of cell density and alignment in the droplet formation, [14], [64] this method invites some novel applications. It is one of the first bioprinting methods to successfully conduct *in vivo* bioprinting. There was a case where mesenchymal stromal cells were used to replace a mouse calvaria, and the print was made directly onto the defective tissue [14]. This method has also been utilized in carcinoma with microvasculature [64], cardiac tissue [50], cellularized skin constructs [50], and adipose tissue [11].

UV-based methods can be divided into three sub categories: stereolithography (SLA), digital light processing (DLP), and digital micromirror devices (DMD) [11], [61], [66], [67]. In all UV-based printing techniques, a print bed is submerged in a liquid photocurable resin, or a bioink in tissue engineering cases. Stimulation by UV light crosslinks the material onto the print bed [5], [20]– [23]. In SLA, a computer-controlled light beam fabricates material vector-by-vector in a bottom-up approach [24]. DLP is where a UV light source is projected onto a transparent surface, within a vat of photosensitive bioink. As a result, the entire layer is crosslinked upon light exposure [20], [23]. Original attempts with DLP included using physical masks applied to the light source to define the pattern for each shape [11], [60], [61], [67].

DMD-based printing is an improvement on the DLP method and thus is a subset of DLP-based bioprinting. In this method, a DMD device provides a dynamic pattern generator allowing for more variability and higher resolution [62], [66]. Within the DMD, thousands of mirrors are precisely controlled through computer aid, which can allow for the light to be reflected in the exact desired pattern, layer-by-layer [55], [62], [66]. This method can result in a precisely defined resolution, achieving in literature as small as 5 μm

in the z-axis [68]. Figure 4 below provides a graphic image for how SLA and DMD-based

DLP bioprinting is achieved [61], [62], [65]–[67].
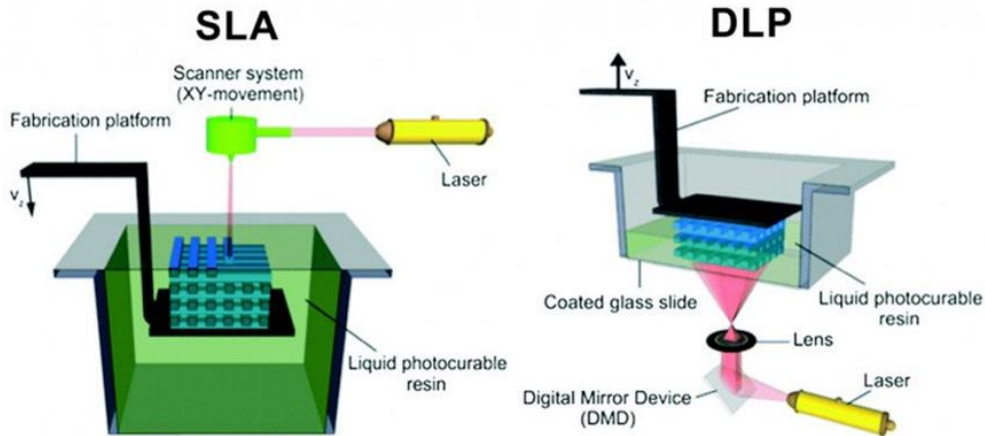
Figure 4. Comparison of SLA and DLP printing methods [68]

Most of these printing systems are configured through a top-down projection.

However, it has been found that a bottom-up projection approach can provide a higher

resolution, material conversation, and quicker print time [52], [69]. This method has a

relatively low cost, good cell viability of (>85 %), and has no limitation of the viscosity of

materials. Typical cell density for this process is $<10^8$ cells/mL [55], [66], [69]. Its speed

is fast comparable to ink injection and is determined by the bioink material and type of

photoinitiator used [11], [59], [69]. These methods have been used in a wide variety of

processes including blood vessel [11], meniscus repair [68], carcinoma [70], [71], and

OOAC [11], [21], [67].

1.5. Bioink Composition

In 3D bioprinting, hydrogels are commonly used to print out these structures. One common biomaterial is GelMA, which is often used as it has a high degree of quality control as well as physical and mechanical properties similar to tissue [58], [72], [73]. In addition, it has been found to be an excellent substrate and has shown successful angiogenesis and cell growth [74]. GelMA is formed with gelatin and methacrylic acid. Gelatin is primarily composed of collagen and elastin monomer chains that are found in most tissues. Since gelatin is thermosensitive, then without any alterations, placing gelatin structures at incubator temperatures (i.e. 37-40 $^{\circ}$C) results in monomer chain relaxation and a liquid state. GelMA presents an altered structure of gelatin. Gelatin and methacrylic acid react to form methacryloyl groups. When a photoinitiator is added to GelMA and it is exposed to UV light, a tangle of the monomers of the gelatin hydrogel matrix is induced that retains tissue-like properties and structure [37], [38], [73], [75], [76]. Typically to replicate human tissue, GelMA ranging from 5-10 wt % is used. The amount of methacrylic acid, source of gelatin, and molecular weight of gelatin have an effect on the viscoelastic properties of the GelMA [77]. This degree of customization allows for precise tuning of the material for bioprinting applications [15], [38], [67], [68], [73]. Other types of naturally-derived polymers can be formed the same way. There has been an emerging use of hyaluronic methacryloyl, either on its own or in conjunction with GelMA, to provide structures that have a higher hyaluronic acid concentration for use with certain tissues [25], [32], [53].

1.5.1. Cell laden bioinks. In 3D cell constructs it is often desirable to have precise patterning for cell culture purposes. The ability to have localized cell positioning, or

equally suspended cells throughout the construct is ideal [11], [73].The main method to achieve this is to prepare bioink that have cells suspended throughout the printing medium. This is often done with soft or thermosensitive materials that can allow for mixing at warmer temperatures, and solidify later through crosslinking. Often, bioinks that are biocompatible are highly desirable to prevent cells from being damaged during the pre-printing and post-printing process. This is necessary for multiculture structures, as multiple bioinks can be prepared that allow studies of processes such as metastasis [11], [17], [78].

1.6. Materials and Methods

1.6.1. Project goals. The overall goal for this model was the development of   an *in vitro* co-culture model. Ideally the model would have replicated the GBM ECM mechanical properties, to study the effect on cell migration and invasion. Customized bioinks and printing parameters that mimic native ECM mechanical properties were developed. This model was a bioprinted microfluidic model composed of a co-culture of GBM cells and endothelial lined channels. The chip was constructed to allow for monitoring in real time of cell migration. The chip was made with a customized DLP bioprinter. The initial goals were for this was to produce a comparable bioink to native ECM, successfully line microfluidic channels with endothelial cells, produce a system that can support co-culture, and to test   a novel bioprinting. At this time the model is a co-culture so without the presence of astrocytes, it lacks the formation seen for the blood brain barrier. In addition, simplified channels were used as leaky vasculature is not considered at this time.

1.6.2. Cell culture. Immortal human glioblastoma cells (U-87: MG cell line, ATCC, USA), cell size range 12–14 μm (B10NUMB3R5: bionumbers.hms.harvard.edu),

were cultured in BD EMEM (Becton, Dickinson and Company, Miami, FL, USA), which was prepared with 10 vol% fetal bovine serum (ATCC 30-2020). Cells were cultured in T75 flasks that were fed every two days and passaged with 1 mL of trypsin-EDTA solution (0.25% Corning, Manassas, VA).

Human umbilical vasculature endothelial cells (HUVECS), cell range 14–15 μm (B10NUMB3R5: bionumbers.hms.harvard.edu), were cultured with an EGMTM-2 Endothelial Cell Growth Medium-2 BulletKitTM (Lonza CC-3162). Cells were seeded in a T75 flask and were fed every two days and passaged with 1 mL of trypsin-EDTA solution (0.25% Corning, Manassas, VA). As a primary cell line was utilized, cells for experiments were used before the 10th passage.

1.6.3. GelMA preparation. Gelatin, 10 g, (Type A from porcine skin, Sigma-Aldrich, G1890) was dissolved into Dulbecco's Phosphate Buffered Saline, DPBS, 100mL (SAFC, Sigma-Aldrich, 56064C) solution by heating on a magnetic stirring plate for h 60°C until the solution was clear and homogenous. Methacrylic anhydride (MA), 8 mL, was added drop-wise into the solution and then heated at 50 °C for one hour. The pre-warmed (40 °C) DPBS was added to the solution, 500 mL, to stop the reaction. Dialysis tubing (12-15 kDA) was cut to a length of 8 in and immersed in deionized (DI) water for 15 min. A knot was made at the end of the tube, and 30 mL of solution was then pipetted into the dialysis tubing until all tubing was filled with solution. Dialysis tubing was placed in DI water for one week at 40 °C, with the water changed twice daily. After a week, solution was collected in a glass flask and sterile filtered (pore size of 0.22 μm). Then 45mL of solution was transferred into a 50 mL Falcon tube and placed in a -80 °C freezer

for 24 h. The solution was prepared for freeze drying and freeze dried for 48 h. It then was stored at -80°C until use.

1.6.4. Bioink preparation. GelMA solution at the desired weight percent was heated in a magnetic stirring plate for 1 hour at 40–60 °C until the solution was clear and homogenous. The solution was sterilized in a biosafety cabinet via a syringe filter (0.2 μm PES, VWR). For bioink preparation, the cells were counted using 20 μL of Trypan Blue Stain (0.4%, EVE, Stretton, UK) and an automated cell counter (RevCount Cell Counter, Oxford, CT, USA). Cell solutions were diluted to the desired cell density by adding pre-warmed gelatin solution. Samples were gently agitated until cell pellets were dispersed through gel solutions.

1.6.5. Rheometer experiments. Rheological measurements were performed using a DHR Hybrid Rheometer (TA Instruments) with a flat-plate geometry measuring system (Plate SST ST 40 MM Smart Swap, Part Number 511400.905, UK), utilizing a parallel-plate geometry. Experiments were performed at 20 °C for the selected cell densities 50 million (M), 5 M, and 0.5 M cells/mL. To ensure that cells were uniformly distributed, solutions were kept in a water bath (37 °C) and each sample was gently agitated before pipetting the sample onto a rheometer plate. The optical opaqueness of gelatin provides a good criterion to assess uniform distributions of cells. Before each test, the samples were cooled to room temperature through the temperature control unit in the rheometer. First was a flow ramp test which measured shear stress (τ, Pa), normal stress (σ, Pa), and steady shear viscosity (η, Pa. s) by changing the shear rate (1 to final 10^3 s^{-1}). Second was an oscillation test (not shown here), conducted using a strain percent of 2%, and a linear sweep angular frequency from 1.0 to 100.0 rad/s to measure the storage

modulus (G′), loss modulus (G″), and phase angle (θ°). Next, the viscosity of a non-Newtonian fluid can be defined by a power law [78]:

$$\eta = K * \gamma^n \tag{1}$$

where γ is the shear rate, K is the viscosity coefficient, and n is the power law index. The parameters K and n can be obtained from the regression of rheological data [78].

1.6.6. Mechanical experiments. Compression tests were carried out with a 100 N force tester with a Shimadzu, EZ-SX Short, (Columbia, MD, USA) machine unit. Compression tests were conducted with a 1 mm thick, 10 mm wide, crosslinked GelMA disc with the Shimadzu compression program at strain rates of 0.1 mm/s.

1.6.7. Live/Dead experiments. The bioink solutions were extruded by hand with a 5 mL syringe with a 25 G needle into a glass container. Live/Dead staining kit was prepared (PromoKine Live/Dead Staining Kit II, Heidelberg Germany) and performed following the standard protocol. Then, the samples were imaged using confocal fluorescence microscopy (Olympus IX-70 with Thorlabs Confocal Microscopy Upgrade, USA). Images were processed with ImageJ (FIJI) software[79].

1.6.8. Statistical analysis. All results were presented as the mean ± standard deviation (SD). Statistical analysis was performed in Microsoft Excel using one-way analysis of variance (ANOVA) in conjugation with a Bonferroni post-hoc test. Three independent trials were carried out unless otherwise stated.

Chapter 2

Mechanical Properties

2.1. Mechanical Properties

Mechanical properties of tissue extracellular matrix (ECM) have a significant impact on the behavior of cells. These mechanical properties are attributed to collagen, elastin, cells, and other biological components that make up the structure of the ECM. To replicate *in vivo* environment, one common material type is water-saturated polymer-like hydrogels [17], [60]. Among different hydrogel systems, GelMA represents a similar composition to human ECM in soft tissues. GelMA over the range of 5-10 wt% prepared with a phosphate buffered saline (PBS) closely replicates human ECM [15], [38], [74], [77].

The mechanical properties of the material selected for printing is very important when having an accurate cellular response. Particularly with tumor tissue, there is an increase in the elastic properties compared to native healthy tissue [80]–[82]. This property has been shown to drive invasiveness and affect cell migration [82].

For our experiments, bioink comprised of cell-laden GelMA was used. There have been extensive studies on the ranges of GelMA correlating to tissue ECM. However, the effect of cell density on the mechanical properties of bioinks in 3D bioprinting has not been extensively explored. The mechanical properties of tissue ECM have a key interaction with GBM. Higher grade tumors seem to experience a change in mechanical properties, as such cell density may also have an effect on the GelMA substrate. To better understand this relationship, shear rheology measurements were conducted on GelMA and culture media-based bioink compositions.

2.2. Rheometer Experiments

2.2.1. Rheometer cell experiments. Intracellular adhesion, colloquially known as the "stickiness" among cells, allows for GBM to invade the smallest spaces within the brain. Samples were prepared in three concentrations of GBM cells suspended in culture media: 50 million cells/mL (50M), 5 million cells/mL (5M), and 500 thousand cells/mL (500K). The rheological tests included: 1) shear force measurements for a sweep of loading frequency, and 2) dynamic viscosity measurements for a range of shear rates. The rheometer tests were conducted at 37 ⁰C to replicate the environment of the human body. The data was collected in the machine software and then represented by three different parameters:

Storage modulus: Material's ability to store elastic energy, E'

Loss modulus: Material's vicious properties, represents amount of energy lost E"

Viscosity: Material's resistance to deformation at a given rate
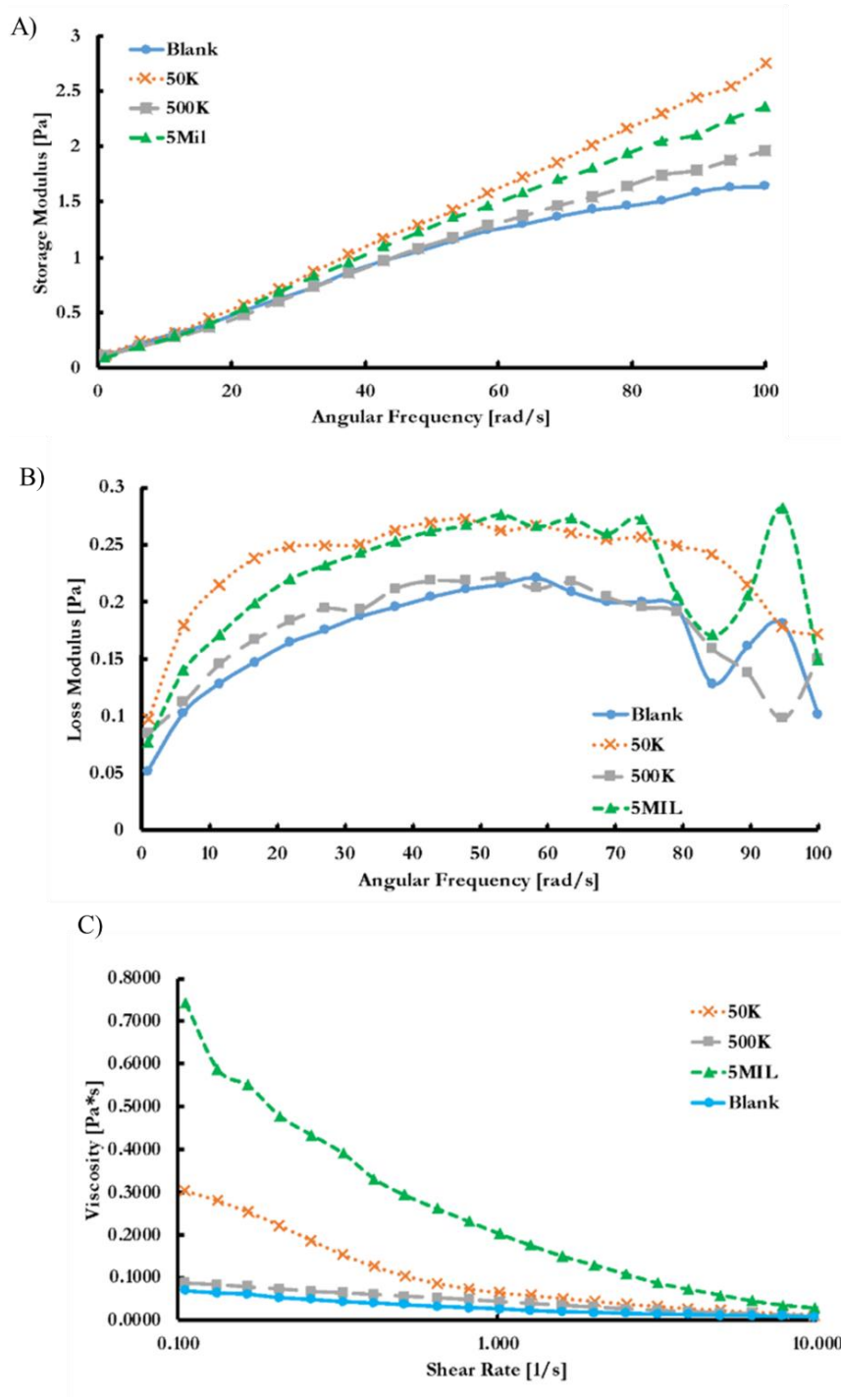
Figure 5. Rheometer data of cell laden media at 37 ℃: A) Storage modulus of cells suspended in media; B) Loss modulus of cells suspended in media; C) Dynamic viscosity of cells suspended in media. All data collected from a dataset of 48 samples.

Compared to basal culture media, the inclusion of cells increases bioink viscosity versus shear rates in a statically significant manner ($p = 0.0096$). This is different for the case of the storage modulus and loss modulus frequency as it was found to not make a large statistical difference between cell laden materials and a control ($p = 0.71$ and $p = 0.65$ respectively for 50K cells/mL). Viscosity under test conditions increases as cell concentration increases; however, loss modulus was not affected by an increase in cell concentration. A visual trend where acellular media was present has the lowest values for viscosity, storage, and loss modulus. As cells were added to media these values increased. 500K cells/mL had the lowest values excluding the acellular media in storage modulus, loss modulus, and viscosity. 50K cells/mL had the highest storage and loss modulus values when compared to the other testing conditions. However, it had a lower viscosity value compared to the 5M testing condition. These observations denote that GBM cells may exhibit viscoelastic properties, with the elastic portion observed at lower angular frequencies. Native brain elasticity increases when glioblastoma affects the tissue; our results show that the cell density within tumors may contribute to the elasticity found in GBM afflicted tissue.

2.2.2. Cell laden bioink experiments. Cell volume, physical cell interactions, viscosity of the matrix, and cell spatial arrangements can impact bioink printability [64], [78]. In order to investigate the role of cells on the shear rheology, experiments were repeated with cell laden GelMA-based bioinks. (Due to preparation costs, we replaced GelMA with gelatin due to their similarity of the physical properties.) GelMA at 7 wt% was used for the rheology experiments. The control, which has no cells present, exhibited the highest values of shear stress and viscosity. As cells were added to the bioink, the

viscosity and shear stress decreased. In addition, a left shift was observed for the shear stress values for cell-laden bioink samples. The lowest values occurred at 5 M cells/mL, and values increased at 50 M cells/mL.

The viscosity data in Figure 6A was then fit to the power law formula and analyzed through linear regression for each cell density test condition. The regression results will be discussed later. Cell volume, physical cell interactions, viscosity of the matrix, and cell spatial arrangements all have an effect on bioink printability [64], [78]. In order to investigate if the same trends occur as observed for media-based bioink, experiments were repeated with GelMA-based bioink. GelMA at 7 wt % was used for the rheology experiments using the same viscometry program as for the cell in media experiments.
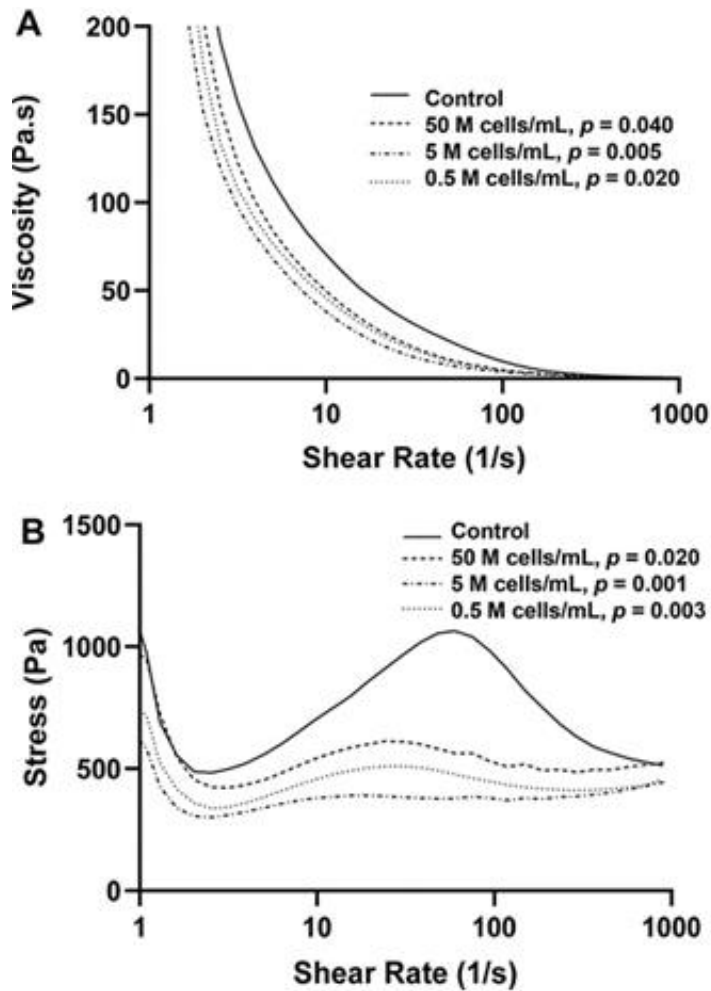
Figure 6. Shear rheology data for cell-laden bioinks (7 wt % gelatin): A) Mean steady shear viscosity versus shear rate (1/s), and B) Mean shear stress versus shear rate (1/s) for different concentrations of U87 cells, where "Control" means 0 cells/mL. Data are averaged from 48 samples. Figure adapted from [78].

Statistical analysis was conducted using ANOVA to determine which testing condition had a higher impact on viscosity and shear stress values. The presence of cells had a statistically significant effect on viscosity and shear stress values. Compared to the control, all cell-laden testing conditions were statistically significant different than the GelMA control condition. As observed in Figure 6, a higher viscosity in the control group was

observed as compared to cell-laden groups. For example, bioink viscosity decreased about 40 % for the cell density of 5 M cells/mL at the shear rate of 10 s−1 (Fig. 6A). The difference between cell-laden and control groups was lessened in the case of 50 M cells/mL (~25 %, p = 0.040). Thus, it was postulated that interactions among cells superseded the void-like weakening mechanism of cells at lower densities. Conclusively, there was a cell density concentration that above the shear-thinning behavior was enhanced and remained nearly constant compared to the control (no cells). The cell density used in 3D bioprinting experiments ranges between 0.5 M and 5 M cells/mL [78]. Many forms of 3D bioprinting resolution depends on the steady shear viscosity of bioinks [55], [83]. Slight viscosity variations can hamper the resolution of bioprinted constructs.

Bioink viscosity depends on the spatial distribution of cells and their interactions with hydrogel precursors [78]. The space among cells and interspace within the hydrogel network was influenced by cell volume. By increasing cell density, the gaps among cells and cell-gel interspace decreased. This affected the behavior of hydrogel systems under physical deformation.

In non-Newtonian viscoelastic solutions, a shift from solid-like behavior occurs when the elastic network breaks up and begins to flow. The shear stress leading to the network dissociation is called yield stress. The yield stress is reached when the shear stress is sufficient to cause the gel network to break up, and after this point the gel behaves like a fluid. The yield stress in gelatin solution was determined to be lowered by cell encapsulation (Fig. 6B). To further investigate this trend, the yield stresses for four concentrations were calculated and summarized in Table 3.

Over 40 % shift in the yield shear stress was observed for the cell-laden bioinks when compared to the control samples. The correlation between the cell density and yield stress is similar to the case of steady shear viscosity. The highest cell density exhibits the highest yield stress among the cell-laden data. This phenomenon can be attributed to the loose connections among neighboring chains as the cells may block their direct contact. This further supports the observation on the rheological data where encapsulating cells act as softening particles. Data has been adapted from published research [78].

Table 3

Linear regression of cell laden bioink viscosity [78]

Density (M cells/mL)	Viscosity Coefficient (Pa. s)	Power Law Index	Yield Stress (kPa)	Injection Force (N)
0	356.52	0.820	1.26 ± 0.45	96.40 ± 3.35
0.5	206.64	0.804	0.79 ± 0.34	83.96 ± 2.65
5	173.73	0.795	0.69 ± 0.07	72.06 ± 4.90
50	225.99	0.798	1.00 ± 0.08	68.69 ± 2.30

2.3. Mechanical Testing of Photo-Crosslinked GelMA

Mechanical testing was conducted under three different testing conditions to represent different GBM disease states. This was executed to confirm if the properties of the prepared 3D constructs were comparable to that of native tissue. An initial selection of 7 wt % GelMA was chosen as a base formula. Prior research had found that between 5-10 wt % was comparable to human tissue [38], [84]. Elastic moduli are dependent on GelMA weight percent composition, UV exposure, percentage of photoinitiator (PI), and level of methacrylation. As such, it is important to confirm if the mechanical properties would be comparable to native tissue of a healthy brain and glioma tissue.

28

Experimental conditions for the three disease states were the following: healthy tissue (7 wt % GelMA + no HA), Mild GBM (7 wt % GelMA + 0.1 wt % HA) and Severe GBM (7 wt % GelMA + 0.05 wt % HA). In this experiment, initial results were tested with a strain rate of 0.01 mm/min to be directly compared to the data collected from patient data [41]. This collected data is summarized in Table 4.

Table 4

Mechanical testing on crosslinked GelMA with and without HA

Sample Name	HA %	Elastic Modulus (kPa)	Strain Rate (mm/s)	Exposure (s)
GelMA Control	0	1.7	0.1	5
Low HA	0.1	24.6	0.1	10
High HA	0.5	3.1	0.1	5
High HA	0.5	4.0	0.1	10

Table 4 shows that the majority of the mechanical property values were not within range of glioblastoma tissue[80]. Experiments were planned for 5, 7, and 10 wt % GelMA at five strain rates of 0.1, 0.3, 0.5, 0.8, and 1 mm/m. The reason for selecting these ranges of values was to determine which parameter had a dominant impact on material properties. Once a basal parametric combination was chosen, HA composition values were to be added and tested. This would show how comparable the hydrogel would be to native tissue. However due to COVID19 evacuation orders during 2020, experiments were halted and could not be completed.

Chapter 3

Bioprinting Parameters

3.1. Initial Bioprinting Experiments

Experiments were executed using a customized DLP printer (Miri Lab). Samples were crosslinked using a ~ 380 nm wavelength light source (light power < 500 mW/cm^2), at 1 mm thick per sample layer (< 5 s exposure time). The printing process led to a 2-D resolution of ~ 20 μm and a maximum fabrication region of 19 mm x 12 mm. A thick single layer configuration was selected in order to allow for sufficient space for cells to be distributed through the crosslinked material. This also minimized the effect of the glass on cell behavior as much as possible. As this was a customized printer setup, a study was conducted to ensure that the different components of printing would have minimal detrimental effect to cell viability. The testing conditions were: material composition, UV wavelength, photoinitiator ratio, and UV excitation energy. To address this, a study was conducted at a few different test conditions to observe and measure the effect on cell viability after printing.

3.2. Photoinitiator (PI) Toxicity

The first experiment conducted in the custom DLP printer tested whether photoinitiator (PI) concentration had an effect on cell viability. Cancer cell line (U87) at a concentration of 500K cells/mL were encapsulated in pre-sterilized GelMA with and without PI. Cells were incubated with both groups for two hours before images were collected by a light

microscope. This was done to allow time for live dead stain to permeate gel and for cells

to settle within the gel.
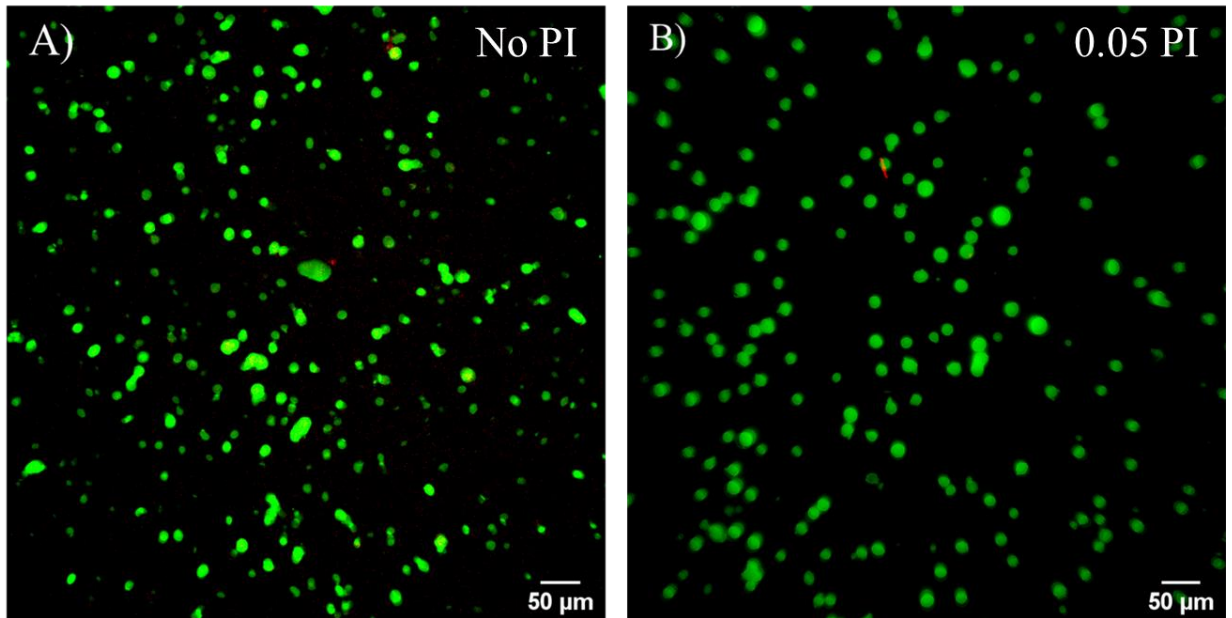
Figure 7. U87 cells after 2 h of exposure to PI: A) 500K cells/mL in GelMA with no PI; B) 500k cells/mL in GelMA with PI concentration of 0.05 wt %

A 0.5 mm depth of each sample was imaged here. In both cases, minimal cell death

was observed (a cell viability of 98%). The PI concentration of 0.05 wt% showed enough

crosslinking and minimal cell death for future experiments.

3.3. Ultraviolet (UV) Exposure Experiments

The next series of experiments consisted of GelMA containing 0.05 wt% photoinitiator

(PI%) exposed to different time periods of ultraviolet (UV) light: 0 s, 100 s, 250 s, 500 s,

750 s, and 1000 s.
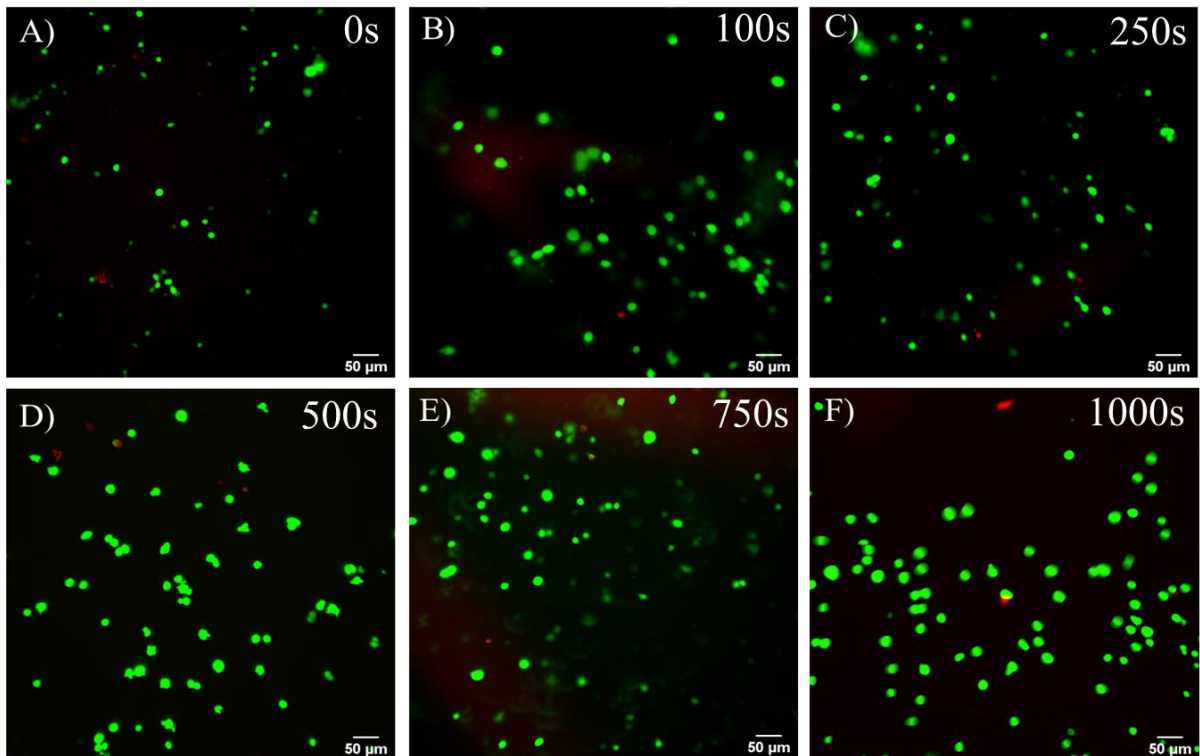
Figure 8. UV wavelength exposure of 500K U87 cells/mL with 0.05 wt % PI at 480 nm, 1 h post-printing: A) No UV exposure, B) 100 s UV exposure time, C) 250 s UV exposure time, D) 500 s UV exposure time, E) 750 s UV exposure time, and F) 1000 s UV exposure time

As observed in Figure 8, each testing condition had a 92 % or greater cell viability, with 1000 s having a 93 % cell viability. Additional experiments were conducted with a lower concentration of PI (0.01 wt %) to see if a lower PI concentration would increase the number of live cells observed compared to the case of 0.05 wt %.

3.4. Concluding Remarks

The bioprinting parameters studied here showed the level of control over the process. There are other parameters that can affect the quality of our OOACs. The current set up

did not include any additional factors such as photo absorbers, or additives such as HA. These will have some impact on how the material crosslinks, in particular photo absorbers have the potential to be cytotoxic to cells depending on the type used. In our OOAC no photo absorbers were used, and the presence of HA has been found to be beneficial to cell growth [31], [55].

The fabrication set up select was the following: ratio of 0.05 wt% PI, 10 s UV exposure, 7 wt% GelMA and 380 nm wavelength as it resulted in very high cell viability. With the experiments conducted, it was concluded that the higher wt% of PI had minimal effect on cell viability so the higher concentration was selected in order to decrease printing time. Cells had minimal death even with very long exposure times (i.e. 1000 s). It was found that the material fully crosslinked for a 1 mm layer within 10 s. Due to this, 10 s exposure was selected to cause the least amount of shock to the cells from environmental factors of ambient temperature.

Chapter 4

Microfluidics-Based Model

4.1. Monoculture Model

Initial tests of monoculture controls were performed to ensure that the methods of cell encapsulation and seeding would cause minimal cell death. To confirm that cells experienced minimal toxicity over a long-term culture, two viability experiments were conducted. U87 cells were cultured in 7 wt % crosslinked GelMA over a period of 8 days. In addition, human vasculature endothelial cells (HUVECs) were seeded in a channel without flow over a period of three days to act as a control for cell behavior in this environment. HUVECs were seeded within a 20G needle channel within a crosslinked GelMA substrate. As this experiment was conducted without a systolic pump, media passively diffused to cells through the porous structure. Due to this there was some concern regarding HUVEC viability after 3 days of no media flow. However, as shown in Figure 9, cells remained within the microfluidic channel and had greater than 80 % cell viability.
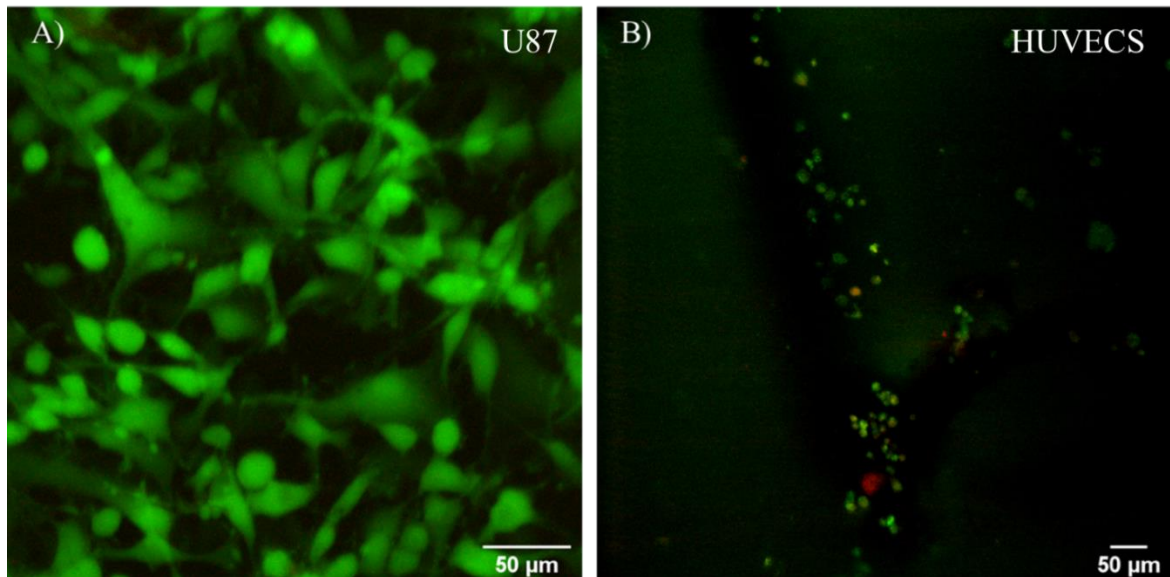
Figure 9. Live/Dead fluorescence microscopy images of monocultures: A) U87 cells cultured over 8 days without flow spread and physically interacted; B) HUVEC cells cultured over 3 days without flow remained spherical. Shear stress needed for formation

4.2. Co-Culture Experiments

Minimal death had occurred with cells in a monoculture environment. In order to explore a multi-culture environment, a 50:50 co-culture of HUVECs and U87 cells over a period of 8 days were conducted. The initial concentration of total cells was 50K cells/mL. In the 50:50 culture conditions, cellular composition consisted of equal concentrations of 25K cells/mL of each cell line. As observed in Figure 10 (B) there appears to be an increase in growth observed in the co-culture when compared to the monoculture of U87. This type of behavior has been observed in other co-culture studies with cancer and HUVEC cell

lines [18]. The presence of HUVEC cells could cause additional proliferation to U87 cells resulting in a higher density.
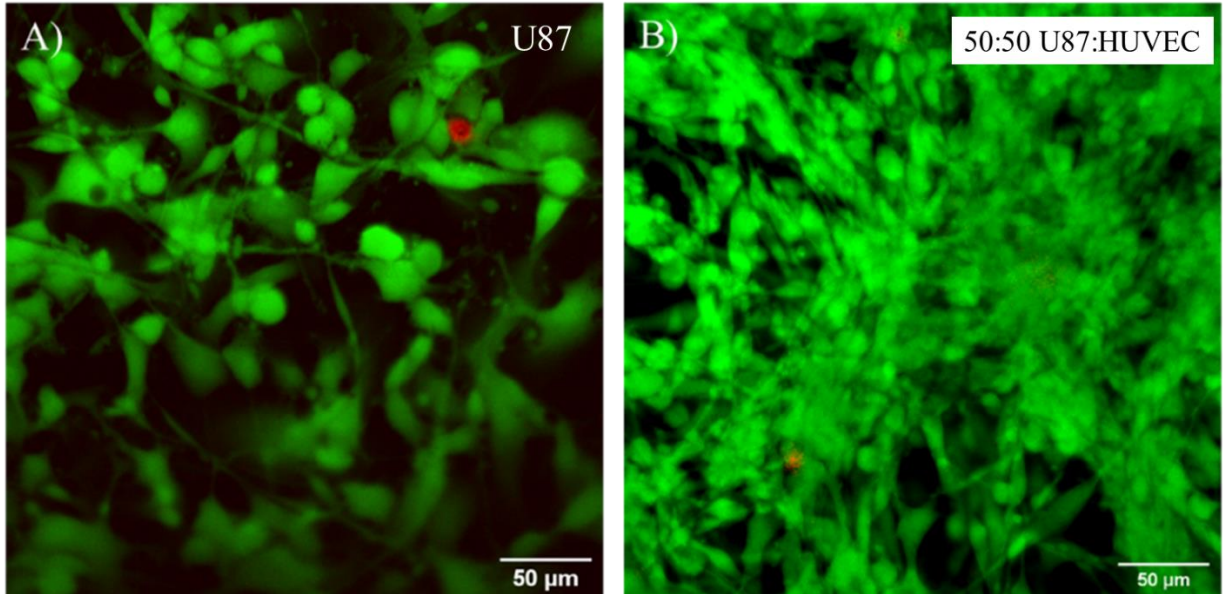
Figure 10. 8-day culturing of 50K cells/mL in 7 wt% GelMA: A) U87, 8-day culture; and B) Co-culture sample of 50:50 U87 and HUVECs over 8 days

4.3. Microfluidic HUVEC Experiments

The cellular behavior in which the cells did not attach to the microfluidic channels is attributed to no-flow conditions. Since shear flow induces attachment of cells in microfluidic channels [16], cellular behavior described above – not attaching in the microfluidic channels – is attributed to no-flow conditions, as shear flow induces attachment of cells in microfluidic channels [16]. The next step was experimentation of seeding cells into a microfluidic channel with multiple days of flow. This was conducted to see how well endothelial cells would spread within the channels, and to determine how much time it would take this to occur *in vitro*. Fibronectin (FN) at 1 wt % was added to

36

channels after printing, and before seeding HUVEC cells at 1M cells/mL. The FN-coated

microfluidic channel system was then hooked up to a systolic pump over a period of days

(3-5).
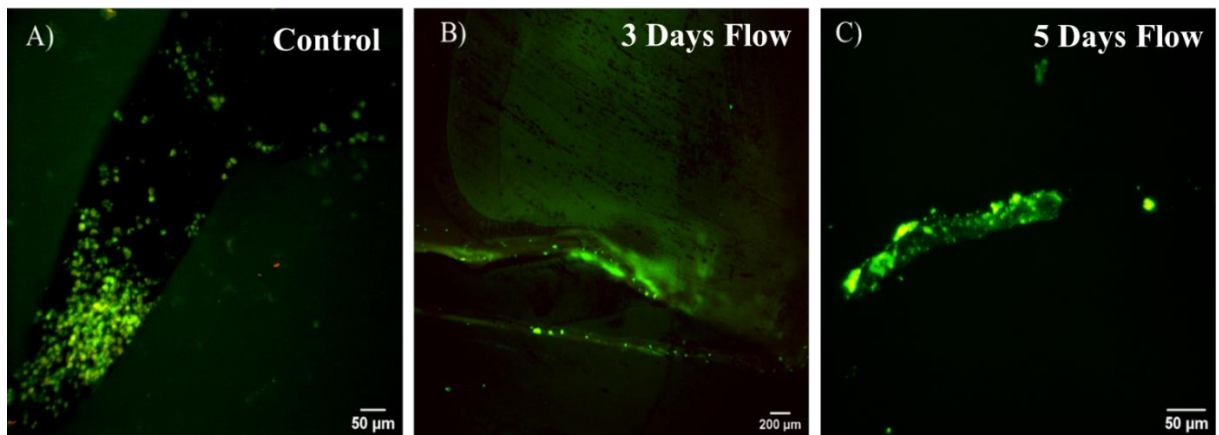
Figure 11. HUVECs seeded in microfluidic channels, with various days of fluid flow: A)
No flow, 5 days; B) Flow, 3 days; C) Flow, 5 days

As observed in Figure 11, as shear flow was introduced, the attachment of the cells

onto the walls of the microfluidic channels occurred. As more time elapsed, more spreading

and further attachments of cells onto the walls of the microfluidic channels were observed.

4.4. Co-Culture Microfluidic Experiments

The next phase of experimentation utilized GMB disease testing conditions as

determined from mechanical property experiments.Three testing conditions with differing

percentages of hyaluronic acid (HA) were selected to represent: healthy brain tissue (0 %

HA), mild gliomas (0.1 % HA), and severe gliomas (0.5% HA). %). Two different

fluorescent tags were selected to tag U87 and HUVECs independently to monitor U87

metastasis towards HUVEC-lined microfluidic channels. The adopted hypothesis was that

as ECM stiffness and HA concentration increased, cellular invasiveness and proliferation would increase, resulting in less time for metastasis to occur. In this case, the higher concentration of HA, or high-grade gliomas, was hypothesized to have the highest level of metastasis. Due to COVID19 evacuations during 2020, experiments were halted in mid-March-2020 and could not be completed at the time of preparing and defending this thesis.

Chapter 5

Conclusions and Future Work

From this research, we have concluded that glioblastoma cells may contribute to the viscoelastic properties of tumors themselves. In addition, in terms of cellularized bioinks comprised of GelMA, we may conclude that there is a critical cell density. At this value, there is a density in which the shear thinning behavior is enhanced and remains nearly constant compared to acellular bioink. This observation was seen with cell densities in the range between 0.5M and 5M cells/mL. Density seems to have an effect on shear mechanical properties however, cell lines may vary where this critical density lies.[78].

We have shown that the customized DLP printer that was developed resulted in minimal cell death during the printing process. This was true even with long UV exposure (1000 s) as there was greater than 90% cell viability. In addition, the bioink and manufacturing composition resulted in high cell viability, verifying the acellular materials of the bioink had minimal impact.

Following literature from past labs [18], [44], a successful co-culture comprising of 50:50 HUVEC and U87 was conducted. From this, we found that co-culture appears to induce GBM proliferation and invasiveness. Current experiments do no show the different cell lines present in the culture, as such two different fluorescent stains to mark each cell line is suggested. In studies from projects with similar co-culture methods [18], [44], similar formation was observed in these initial experiments. This behavior of infusion and attachment has been seen in other co-culture cancer models [18], [54].

It was planned to have three testing conditions exhibiting mechanical properties from different levels of glioblastoma disease progression (health brain, low-grade glioma, high grade glioma) [39]. It has been shown in literature HA concentration increases as gliomas get more severe, which in turn induces invasiveness of glioblastoma [24], [27]. Additional mechanical testing is advised in order to have comparable synthetic ECM mechanical properties. This can be done by adjusting the crosslinking time and wt% of GelMA. As HA can be produced by cells and would be hard to correlate exact amounts to *in vivo* it is advised to keep the HA wt% the same as initial experiments presented. This is to have a replicable synthetic ECM environment to what is seen *in vivo*.

Before the development of the organ-on-a-chip platform, additional tests are suggested for the endothelial lined microfluidic channels. An actin and DAPI stain is suggested in order to see the location of the cell envelope and location of the endothelial cells in the cell lined channels. In addition, a perfusion test is suggested as a secondary test to ensure an endothelial barrier is formed. In order to build a better model, it is suggested that monitoring shear flow, initial cell density, and how long the channel takes to form should be noted in order to ensure the barrier is formed before GBM cells are introduced in a co-culture model. Further experimentation on bioink ECM properties should be conducted in order to create a comparable ECM to forms of the GBM environment. After these bioinks and printing parameters are verified, a migration study can be conducted. This is done by having an initial tumor location of GBM cells and a HUVEC lined microfluidic channel in a co-culture microfluidic system. Monitoring cell line interactions would be done by staining each cell line with a different fluorescent stain and monitoring the migration and time it takes for the GBM cells to reach a HUVEC lined channel. It is hypothesized that

higher elastic modulus and higher HA concentration should result in more invasive behavior to occur within a shorter time frame.

Due to COVID 19, many of these additional and planned experiments could not be completed and had to be halted due to the current pandemic at the time of this thesis.

References

[1]   R. L. Siegel, K. D. Miller, and A. Jemal, "Cancer Statistics, 2018," *CA: a Cancer Journal for Clinicians*, vol. 69, no. 1, pp. 7–34, 2019.

[2]   M. C. Barcellos-Hoff, Mary Hellen.; B. Sumru, D. Bready and E. Al., *Glioblastoma-Methods and Protocols*, 1st ed. New York, 2018.

[3]   D. Krivosheya *et al.*, *Advances in Biology and Treatment of Glioblastoma*, 1st ed. Cham, Switzerland: Springer, 2017.

[4]   W. I. Cancer, "What is Cancer?," *American Cancer Society*, 2015. .

[5]   Startonology, "Central Nervous System Gliomas – 2017," *Startonology Europe*, 2017. .

[6]   H. Setia and A. R. Muotri, "Seminars in Cell & Developmental Biology Brain Organoids as a Model System for Human Neurodevelopment and Disease," *Seminars in Cell and Developmental Biology*, vol. 95, no. August 2018, pp. 93–97, 2019.

[7]   H. H. Hwang, W. Zhu, G. Victorine, N. Lawrence, and S. Chen, "3d Printing: 3D-Printing of Functional Biomedical Microdevices via Light- and Extrusion-Based Approaches (Small Methods 2/2018)," *Small Methods*, vol. 2, no. 2, p. 1870021, 2018.

[8]   A. K. Miri, E. Mostafavi, D. Khorsandi, S. Hu, M. Malpica, and A. Khademhosseini, "Bioprinters for Organs-on-Chips," *Biofabrication*, vol. 11, no. 042002, pp. 1–15, 2019.

[9]   S. P. Deosarkar, B. Prabhakarpandian, B. Wang, J. B. Sheffield, B. Krynska, and M. F. Kiani, "A Novel Dynamic Neonatal Blood-Brain Barrier on a Chip," *PLOS One*, pp. 1–21, 2015.

[10]   M. Ali, M. Jahromi, A. Abdoli, M. Rahmanian, and H. Bardania, "Microfluidic Brain-on-a-Chip : Perspectives for Mimicking Neural System Disorders," *Molecular Neurobiology*, vol. 56, pp. 8489–8512, 2019.

[11]   C. Mandrycky, Z. Wang, K. Kim, and D. H. Kim, "3D Bioprinting for Engineering Complex Tissues," *Biotechnology Advances*, vol. 34, no. 4, pp. 422–434, 2016.

[12]   D. Loessner *et al.*, "Functionalization, Preparation and Use of Cell-Laden Gelatin Methacryloyl-Based Hydrogels as Modular Tissue Culture Platforms," *Nature Protocols*, vol. 11, no. 4, pp. 727–746, 2016.

[13]   Y. Zhao *et al.*, "Three-Dimensional Printing of Hela Cells for Cervical Tumor Model In Vitro," *Biofabrication*, vol. 6, no. 3, 2014.

[14]   V. Keriquel *et al.*, "In Situ Printing of Mesenchymal Stromal Cells, by Laser-Assisted Bioprinting, for In Vivo Bone Regeneration Applications," *Scientific Reports*, vol. 7, no. 1, pp. 1–11, 2017.

[15] G. Gao *et al.*, "Improved Properties of Bone and Cartilage Tissue From 3D Inkjet-Bioprinted Human Mesenchymal Stem Cells by Simultaneous Deposition and Photocrosslinking in PEG-GelMA," *Biotechnology Letters*, vol. 37, no. 11, pp. 2349–2355, 2015.

[16] A. K. Miri, A. Khalilpour, B. Cecen, S. Maharjan, S. R. Shin, and A. Khademhosseini, "Multiscale Bioprinting of Vascularized Models," *Biomaterials*, vol. 198, no. May 2018, pp. 204–216, 2019.

[17] I. T. Ozbolat and M. Hospodiuk, "Current Advances and Future Perspectives in Extrusion-Based Bioprinting," *Biomaterials*, vol. 76, pp. 321–343, 2016.

[18] M. F. Coughlin and R. D. Kamm, "The Use of Microfluidic Platforms to Probe the Mechanism of Cancer Cell Extravasation," *Advanced Healthcare Materials*, vol. 9, no. 1901410, pp. 1–15, 2020.

[19] I. Manini *et al.*, "Role of Microenvironment in Glioma Invasion : What We Learned from In Vitro Models," *Internation Journal of Molecular Sciences*, vol. 19, no. 147, pp. 1–32, 2017.

[20] V. A. Cuddapah, S. Robel, S. Watkins, and H. Sontheimer, "A Neurocentric Perspective on Glioma Invasion," *Nature Publishing Group*, vol. 15, no. 7, pp. 455–465, 2014.

[21] F. Meng, C. M. Meyer, D. Joung, D. A. Vallera, M. C. McAlpine, and A. Panoskaltsis-Mortari, "3D Bioprinted In Vitro Metastatic Models via Reconstruction of Tumor Microenvironments," *Advanced Materials*, vol. 31, no. 10, pp. 1–10, 2019.

[22] Q. T. Ostrom *et al.*, "Neuro-Oncology CBTRUS Statistical Report : Primary Brain and Other Central Nervous System Tumors Diagnosed in the United States in 2012-2016," *Neuro-Oncology*, vol. 21, no. S5, pp. 1–100, 2019.

[23] Y. Fan, D. T. Nguyen, Y. Akay, F. Xu, and M. Akay, "Engineering a Brain Cancer Chip for High-Throughput Drug Screening," *Nature Publishing Group*, vol. 6, no. 25062, pp. 1–13, 2016.

[24] J. Cha and P. Kim, "Biomimetic Strategies for the Glioblastoma Microenvironment," *Frontiers in Materials*, vol. 4, no. December, pp. 1–8, 2017.

[25] J. E. Chen, S. Pedron, P. Shyu, Y. Hu, J. N. Sarkaria, and B. A. C. Harley, "Influence of Hyaluronic Acid Transitions in Tumor Microenvironment on Glioblastoma Malignancy and Invasive Behavior," *Frontiers in Materials*, vol. 5, no. June, pp. 1–11, 2018.

[26] I. Levental, C. Georges, and P. A. Janmey, "Soft Biological Materials and Their Impact on Cell Function," *Soft Matter*, vol. 3, pp. 299–306, 2007.

[27] G. Fricker *et al.*, *The Blood Brain Barrier (BBB)*, 1st ed. London, 2014.

[28] B. Engelhardt and S. Liebner, "Novel Insights Into the Development and Maintenance of the Blood – Brain Barrier," *Cell Tissue Research*, vol. 355, pp. 687–699, 2014.

[29] Y. Kim and S. Kumar, "CD44-Mediated Adhesion to Hyaluronic Acid Contributes to Mechanosensing and Invasive Motility," *Molecular Cancer Research*, vol. 12, no. October, pp. 1416–1430, 2014.

[30] E. Metastasis and P. Central, "CD44 Expression and Hyaluronic Acid Binding of Malignant Glioma Cells," *Clinical & Experimental Metastasis*, vol. 17, pp. 71–76, 1999.

[31] J. B. Park, H. Kwak, S. Lee, J. B. Park, H. Kwak, and S. Lee, "Role of Hyaluronan in Glioma Invasion," *Cell Adhesion & Migration*, vol. 2, no. 3, pp. 202–207, 2008.

[32] D. R. Z. M. T. Dours-zimmermann, "Extracellular Matrix of the Central Nervous System : From Neglect to Challenge," *Histochem Cell Biology*, vol. 130, pp. 635–653, 2008.

[33] J. D. et al Wolf, K.J, Chen, J., Coombes, "Dissecting and Rebuilding the Glioblastoma Microenviroment with Engineered Materials," *Nature Review Material*, vol. 4, pp. 651–668, 2019.

[34] S. Jin *et al.*, "The Effect of Hyaluronic Acid on the Invasiveness of Malignant Glioma Cells : Comparison of Invasion Potential at Hyaluronic Acid Hydrogel and Matrigel," pp. 472–478, 2009.

[35] J. Liu, M. Hofmann, M. Hamou, and N. De Tribolet, "Differential CD44 Expression Patterns in Primary Brain Tumours and Brain Metastases," *British Journal of Cancer*, vol. 72, no. 135, pp. 160–163, 1995.

[36] C. Wang, X. Tong, and F. Yang, "Bioengineered 3D Brain Tumor Model to Elucidate the Effects of Matrix Stiffness on Glioblastoma Cell Behavior Using PEG-Based Hydrogels," *Molecular Pharmaceutics*, vol. 11, pp. 2115–2125, 2014.

[37] R. Gauvin *et al.*, "Microfabrication of Complex Porous Tissue Engineering Scaffolds Using 3D Projection Stereolithography," *Biomaterials*, vol. 33, no. 15, pp. 3824–3834, 2012.

[38] A. Tamayol, N. Annabi, and A. Khademhosseini, "Biomaterials Synthesis , Properties , and Biomedical Applications of Gelatin Methacryloyl (GelMA) Hydrogels," *Biomaterials*, vol. 73, no. 2015, pp. 254–271, 2020.

[39] T. Lam *et al.*, "Photopolymerizable Gelatin and Hyaluronic Acid for Stereolithographic 3D Bioprinting of Tissue-Engineered Cartilage," *Journal of Biomedical Materials Research - Part B Applied Biomaterials*, pp. 1–9, 2019.

[40] B. H. Rath, J. M. Fair, M. Jamal, K. Camphausen, and P. J. Tofilon, "Astrocytes Enhance the Invasion Potential of Stem-Like Cells," *PLOS One*, vol. 8, no. 1, pp. 1–11, 2013.

[41] J. A. W. Van Dommelen, T. P. J. Van Der Sande, M. Hrapko, and G. W. M. Peters, "Mechanical Properties of Brain Tissue by Indentation : Interregional Variation," *Journal of the Mechanical Behavior of Biomedical Materials*, vol. 3, no. 2, pp. 158–166, 2010.

[42] R. Daneman and A. Prat, "The Blood –Brain Barrier," *Cold Spring Harbor Perspectives in Biology*, vol. 7, pp. 1–23, 2015.

[43] J. Keaney and M. Campbell, "The Dynamic Blood – Brain Barrier," *The FEBS Journal*, vol. 282, pp. 4067–4079, 2015.

[44] S. Wei *et al.*, "Modeling Nanocarrier Transport Across a 3D In Vitro Human Blood-Brain-Barrier Microvasculature," *Advanced Healthcare Materials*, vol. 9, no. 1901486, pp. 1–12, 2020.

[45] R. Kollath, "Bauer-Hartz Blood Brain Barrier Group: Capillary Cross Section," *Kollath Graphic Design*, 2020. [Online]. Available: https://kollathdesign.com/portfolio/university-of-minnesota-college-of-pharmacy-duluth-capillary-cross-sectio/. [Accessed: 05-Apr-2020].

[46] F. Bonnier *et al.*, "Cell Viability Assessment Using the Alamar Blue Assay: A Comparison of 2D and 3D Cell Culture Models," *Toxicology in Vitro*, vol. 29, no. 1, pp. 124–131, 2015.

[47] C. Lee, E. Abelseth, L. de la Vega, and S. M. Willerth, "Bioprinting a Novel Glioblastoma Tumor Model Using a Fibrin-Based Bioink for Drug Screening," *Materials Today Chemistry*, vol. 12, pp. 78–84, 2019.

[48] S. S. Stylli, R. B. Luwor, T. M. B. Ware, F. Tan, and A. H. Kaye, "Mouse Models of Glioma," *Journal of Clinical Neuroscience*, vol. 22, no. 4, pp. 619–626, 2015.

[49] S. Afewerki, A. Sheikhi, S. Kannan, S. Ahadian, and A. Khademhosseini, "Gelatin-polysaccharide Composite Scaffolds for 3D Cell Culture and Tissue Engineering : Towards Natural Therapeutics," *AIChE Bioengineering and Translational Medicine*, vol. 4, pp. 96–115, 2019.

[50] X. Zhang and Y. Zhang, "Tissue Engineering Applications of Three-Dimensional Bioprinting," *Cell Biochemistry and Biophysics*, vol. 72, no. 3, pp. 777–782, 2015.

[51] D. Wu and C. Xu, "Predictive Modeling of Droplet Formation Processes in Inkjet-Based Bioprinting," *Journal of Manufacturing Science and Engineering*, vol. 140, no. 10, p. 101007, 2018.

[52] D. Han, Z. Lu, S. A. Chester, and H. Lee, "Micro 3D Printing of a Temperature-Responsive Hydrogel Using Projection Micro-Stereolithography," *Scientific Reports*, vol. 8, no. 1, pp. 1–11, 2018.

[53] S. Jung *et al.*, "Brain Tumor Invasion Model System Using Organotypic Brain-Slice Culture as an Alternative to In Vivo Model," *Journal Cancer Research Clinical Oncology*, vol. 128, pp. 469–476, 2002.

[54] R. K. W. Polacheck, I. Zervantonakis, "Tumor Cell Migration in Complex Microenvironments," *Cellular and Molecular Life Sciences*, vol. 70, pp. 1335–1356, 2013.

[55] A. K. Miri, A. Khalilpour, B. Cecen, S. Maharjan, S. R. Shin, and A. Khademhosseini, "Multiscale Bioprinting of Vascularized Models," *Biomaterials*, vol. 198, no. August, pp. 204–216, 2019.

[56] T. B. T. Hall, A. G. Ammer, J. I. G. Griffith, and P. R. Lockman, "Permeability Across a Novel Microfluidic Blood - Tumor Barrier Model," *Fluids and Barriers of the CNS*, vol. 14, no. 3, pp. 1–11, 2017.

[57] M. K. Gupta *et al.*, "3D Printed Programmable Release Capsules," *Nano Letters*, vol. 15, no. 8, pp. 5321–5329, 2015.

[58] J. Schöneberg *et al.*, "Engineering Biofunctional in Vitro Vessel Models Using a Multilayer Bioprinting Technique," *Scientific Reports*, vol. 8, no. 1, pp. 1–14, 2018.

[59] I. T. Ozbolat, K. K. Moncal, and H. Gudapati, "Evaluation of Bioprinter Technologies," *Additive Manufacturing*, vol. 13, pp. 179–200, 2017.

[60] J. Gopinathan and I. Noh, "Recent Trends in Bioinks for 3D Printing," *Biomaterials Research*, vol. 22, no. 1, pp. 1–15, 2018.

[61] K. Kowsari *et al.*, "Photopolymer Formulation to Minimize Feature Size, Surface Roughness, and Stair-stepping in Digital Light Processing-based Three-dimensional Printing," *Additive Manufacturing*, vol. 24, no. July, pp. 627–638, 2018.

[62] C. Sun, N. Fang, D. M. Wu, and X. Zhang, "Projection Micro-Stereolithography Using Digital Micro-Mirror Dynamic Mask," *Sensors and Actuators, A: Physical*, vol. 121, no. 1, pp. 113–120, 2005.

[63] Z. Wang *et al.*, "Visible Light Photoinitiation of Cell-Adhesive Gelatin Methacryloyl Hydrogels for Stereolithography 3D Bioprinting," *ACS Applied Materials and Interfaces*, vol. 10, no. 32, pp. 26859–26869, 2018.

[64] B. Guillotin *et al.*, "Laser Assisted Bioprinting of Engineered Tissue with High Cell Density and Microscale Organization," *Biomaterials*, vol. 31, no. 28, pp. 7250–7256, 2010.

[65] R. Pires, "Blinded by the Light DLP vs SLA – 3D Printing Technologies Shootout," *all3dp*, 2019. .

[66] T. Yoon, C. S. Kim, K. Kim, and J. ryul Choi, "Emerging Applications of Digital Micromirror Devices in Biophotonic Fields," *Optics and Laser Technology*, vol. 104, pp. 17–25, 2018.

[67] A. K. Miri *et al.*, "Microfluidics-Enabled Multimaterial Maskless Stereolithographic Bioprinting," *Advanced Materials*, vol. 30, no. 27, pp. 1–9, 2018.

[68] S. P. Grogan *et al.*, "Digital Micromirror Device Projection Printing System for Meniscus Tissue Engineering," *Acta Biomaterialia*, vol. 9, no. 7, pp. 7218–7226, 2013.

[69] S. A. Skoog, P. L. Goering, and R. J. Narayan, "Stereolithography in Tissue Engineering," *Journal of Materials Science: Materials in Medicine*, vol. 25, no. 3, pp. 845–856, 2014.

[70] W. Zhu *et al.*, "Rapid Continuous 3D Printing of Customizable Peripheral Nerve Guidance Conduits," *Materials Today*, vol. 21, no. 9, pp. 951–959, 2018.

[71] X. Ma *et al.*, "Rapid 3D Bioprinting of Decellularized Extracellular Matrix with Regionally Varied Mechanical Properties and Biomimetic Microarchitecture," *Biomaterials*, vol. 185, no. July, pp. 310–321, 2018.

[72] M. Costantini, S. Testa, E. Fornetti, A. Barbetta, and C. Gargioli, "Engineering Muscle Networks in 3D Gelatin Methacryloyl Hydrogels: Influence of Mechanical Stiffness and Geometrical Confinement," *Frontiers in Bioengineering and Biotechnology*, vol. 5, no. Article 22, pp. 1–8, 2017.

[73] D. Loessner *et al.*, "Functionalization , Preparation and Use of Cell-Laden Gelatin Methacryloyl – Based Hydrogels as Modular Tissue Culture Platforms," *Nature Protocols*, vol. 11, no. 4, pp. 727–746, 2016.

[74] H. Stratesteffen, M. Köpf, F. Kreimendahl, A. Blaeser, S. Jockenhoevel, and H. Fischer, "GelMA-Collagen Blends enable Drop-On-Demand 3D Printability and Promote Angiogenesis," *International Society for Biofabrication*, vol. 9, no. 045002, pp. 1–13, 2017.

[75] E. Pagès, M. Rémy, V. Kériquel, M. M. Correa, B. Guillotin, and F. Guillemot, "Creation of Highly Defined Mesenchymal Stem Cell Patterns in Three Dimensions by Laser-Assisted Bioprinting," *Journal of Nanotechnology in Engineering and Medicine*, vol. 6, no. 2, p. 021006, 2015.

[76] E. Hoch, C. Schuh, T. Hirth, E. M. Tovar, and K. Borchers, "Stiff Gelatin Hydrogels Can be Photo-chemically Synthesized from Low Viscous Gelatin Solutions Using Molecularly Functionalized Gelatin with a High Degree of Methacrylation," *Journal of Material Medicine*, vol. 23, pp. 2607–2617, 2012.

[77] K. Rahali *et al.*, "Synthesis and Characterization of Nanofunctionalized Gelatin Methacrylate Hydrogels," *International Journal of Molecular Sciences*, vol. 18, no. 2675, pp. 1–18, 2017.

[78] R. Schwartz, M. Malpica, G. L. Thompson, and A. K. Miri, "Cell Encapsulation in Gelatin Bioink Impairs 3D Bioprinting Resolution," *Journal of the Mechanical Behavior of Biomedical Materials*, vol. 103, 2020.

[79] J. Schindelin, I. Arganda-Carreras, and E. Fries, "Fiji: an open-source platform for biological-image analysis," *Nature methods*, vol. 9, no. 7, pp. 676–682, 2012.

[80] M. T. et al. D. Chauvet, M. Imbault, "In Vivo Measurement of Brain Tumor Elasticity Using Intraoperative Shear Wave Elastography," *Ultraschall in Medicine*, no. 37, pp. 584–590, 2016.

[81] V. B. Morris, S. Nimbalkar, M. Younesi, P. McClellan, and O. Akkus, "Mechanical Properties, Cytocompatibility and Manufacturability of Chitosan:PEGDA Hybrid-Gel Scaffolds by Stereolithography," *Annals of Biomedical Engineering*, vol. 45, no. 1, pp. 286–296, 2017.

[82] V. Umesh, A. D. Rape, T. A. Ulrich, and S. Kumar, "Microenvironmental Stiffness Enhances Glioma Cell Proliferation by Stimulating Epidermal Growth Factor Receptor Signaling," *PLOS One*, vol. 9, no. 7, pp. 1–9, 2014.

[83] Y. Zhou *et al.*, "Coaxial Extrusion Bioprinting of 3D Microfibrous Constructs With Cell-Favorable Gelatin Methacryloyl Microenvironments," *Biofabrication*, vol. 10, no. 2, p. 024102, 2017.

[84] A. K. Miri, H. Goodarzi, B. Cecen, and S. Hassan, "Acta Biomaterialia Permeability Mapping of Gelatin Methacryloyl Hydrogels," *Acta Biomaterialia*, vol. 77, pp. 38–47, 2018.